Piezo1 mechanosensing regulates integrin-dependent chemotactic migration in human T cells

Chinky Shiu Chen Liu[1], Tithi Mandal[2], Parijat Biswas[3], Md. Asmaul Hoque[1,4], Purbita Bandopadhyay[1,4], Bishnu Prasad Sinha[1,4], Jafar Sarif[1,4], Ranit D'Rozario[1,4], Deepak Kumar Sinha[3], Bidisha Sinha[2], Dipyaman Ganguly[1]*

[1]IICB-Translational Research Unit of Excellence, CSIR-Indian Institute of Chemical Biology, Kolkata, India.

[2]Department of Biological Sciences, Indian Institute of Science Education and Research, Kolkata, India.

[3] Department of Biological Sciences, Indian Association for Cultivation of Science, Kolkata, India.

[4]Academy of Scientific and Innovative Research, Ghaziabad, India.

Correspondence: dipyaman@iicb.res.in

Running title: Piezo1 mechanosensing in human T cell chemotaxis

Keywords: Human T cells, Piezo1, Mechanosensing, Migration, Chemokine, Chemotaxis, Focal adhesion kinase, LFA-1, F-actin, Confocal Microscopy, Interference Reflection Microscopy

ABSTRACT

T cells are crucial for efficient antigen-specific immune responses and thus their migration within the body, to inflamed tissues from circulating blood or to secondary lymphoid organs, play a very critical role. T cell extravasation in inflamed tissues depends on chemotactic cues and interaction between endothelial adhesion molecules and cellular integrins. A migrating T cell is expected to sense diverse external and membrane-intrinsic mechano-physical cues, but molecular mechanisms of such mechanosensing in cell migration are not established. We explored if the professional mechanosensor Piezo1 play any role during integrin-dependent chemotaxis of human T cells. We found that deficiency of Piezo1 in human T cells interfered with integrin-dependent cellular motility on ICAM-1-coated surface. Piezo1 recruitment at the leading edge of moving T cells is dependent on and follows focal adhesion formation at the leading edge and local increase in membrane tension on chemokine receptor activation. Piezo1 recruitment and activation, followed by calcium influx and calpain activation, in turn are crucial for the integrin LFA-1 recruitment at the leading edge of the chemotactic human T cells. Thus we find that Piezo1 activation in response to local mechanical cues constitutes a membrane-intrinsic component of the 'outside-in' signaling in human T cells, migrating in response to chemokines, that mediates integrin recruitment to the leading edge.

INTRODUCTION

Efficient T cell migration from blood circulation to secondary lymphoid organs and inflamed tissue is paramount for optimal tissue antigen sampling and effector functions during adaptive immune response (1-4). The process is dependent on chemotactic cues, interaction between endothelial adhesion molecules and T cell integrins, and an intricate acto-myosin dynamics (5). Generation of mechanical force is critical to propel migrating cells (6-9). Mechanosensing of the substrate and increase in cellular membrane tension is also intuitively apparent in a migrating T cell, although mechanistic details are not explored to a great extent.

Piezo1 and Piezo2 ion channels are evolutionarily conserved professional mechanosensors that can sense increase in membrane tension mostly independent of other protein-protein interactions (10-12). Mechanosensing by Piezo1 has been demonstrated to play critical role in diverse patho-physiologic contexts given its wide tissue expression including the immunocellular compartment (13-21). We previously identified crucial role of this specialized mechanotransducer in optimal TCR triggering (14, 19). The immunocellular expression of Piezo1 thus makes it a strong candidate for mechanosensing at the plasma membrane to regulate motility of immune cells. Piezo1 shows differential involvement in cellular migration depending on context (22- 28). Previous studies point to the possibility of a role of Piezo1 in confinement sensing and integrin activation in moving cells, while it deters integrin-independent cell motility, usually referred to as amoeboid movement (29, 30).

Here we aimed at exploring if Piezo1 mechanosensing plays any role during integrin-dependent chemotactic migration of human T cell migration, a patho-physiologically critical event in an ongoing immune response as well as in the steady-state. We found that deficiency of Piezo1 expression in human $CD4^+$ T cells as well as Jurkat T cells interfered with efficient integrin-dependent cellular motility in response to a chemotactic cue. We also found that Piezo1 activation constitutes a hitherto unknown membrane-intrinsic component of the 'outside-in' signaling in human T cells in response to chemokine receptor activation, that follows activation of focal adhesion kinase leading to local increase in membrane tension and mediates local recruitment of integrin molecules at the leading edge of the moving human T cells.

RESULTS

Piezo1 deficiency abrogates integrin-dependent chemotactic motility in human T cells

67 We first assessed the role of Piezo1 on integrin-dependent, non-directional motility of primary
68 human $CD4^+$ T cells. We used GFP plasmid and Piezo1 siRNA co-transfected cells to facilitate
69 distinction between potentially transfected and untransfected cells during cell tracking. We
70 compared the motility of GFP^+ T cells (presuming they had a good transfection efficiency and thus
71 will also have the siRNA) with the GFP^- T cells in the same culture. This was confirmed by flow
72 cytometric assessment of Piezo1 protein content on the T cell surface as well as the whole T cells
73 (Supplemental figures 1B, C). Piezo1 deficiency in T cells (potentially GFP^+) significantly hindered
74 their migration in response to CCL19 in terms of its mean-squared displacement (MSD, Figure 1A-C).
75 Representative cell tracks of Piezo1 deficient (GFP^+) and control (GFP^-) are shown in Figure 1B and
76 Supplementary Figure 1D.

77 ICAM1-coated transwell chemotaxis assay of human $CD4^+$ T lymphocytes and Jurkat T cells also
78 showed significant reduction in migration upon siRNA-mediated Piezo1 knockdown, in response to
79 CCL19 and SDF1α gradients, respectively (Figure. 1D, E). Piezo1 inhibition with GsMTx4 also led to
80 significant impairment of transwell chemotaxis (Supplementary figure 1E).

81

82 **Redistribution of Piezo1 toward the leading edge of migrating T cells in response to chemotactic**
83 **cue**

84 Cell polarity is a crucial aspect of directional cell motility in response to chemokines. $CD4^+$ T cells
85 seeded on ICAM-1 bed showed striking polarity in Piezo1 distribution, upon stimulation with CCL19
86 for 15 minutes (Figure 1F, G; Supplemental video 1). Piezo1 m-Cherry expressing Jurkat T cells also
87 showed striking leading edge polarity in the presence of SDF1α under ICAM1 adhesion (Figure 1H).
88 In Figure 1I, particle image velocimetry (PIV) analysis of a single representative Jurkat cell has been
89 shown to display the dynamically polarized Piezo1 fluorescence upon SDF1α treatment with time, as
90 opposed to rather uniformly distributed Piezo1 signals in a representative untreated cell. The
91 continuous redistribution of Piezo1 within the motile T cells towards the leading edge can also be
92 appreciated in the representative moving image provided (Supplemental video 2).

93

94 **Piezo1 redistribution in migrating T cells follow increased membrane tension in the leading edge**

95 Piezo1 is a professional mechanosensor ion channel, which senses increase in plasma membrane
96 tension and responds by driving calcium influx into the cells (14, 19, 31). As T cells migrate on
97 substrate by extending membrane processes, it is intuitive to hypothesize that a component of

98 mechanosensing is incorporated in the mechanism of cellular movement. The data above, on a
99 critical role of Piezo1 in migrating human T cells, also led us to hypothesize that Piezo1
100 mechanosensors may play a role in sensing mechanical cues in a moving T cell. So, first we aimed at
101 confirming that there is polarized increase in tension in the leading edge plasma membrane of
102 human T cells, moving in response to a chemotactic cue.

103 Cellular membrane tension can be measured by various techniques. However, most of the usual
104 techniques, viz. atomic force microscopy or tension measurement using optical tweezers, are
105 invasive and interfere with the membrane dynamics, as well as are difficult to employ on moving
106 cells. We utilized the non-invasive technique of interference reflection microscopy or IRM for
107 studying potential redistribution of membrane tension following chemokine stimulation (32, 33). In
108 IRM technique, steady-state local fluctuations in the plasma membrane is imaged in cells adhered to
109 a glass coverslip. The interference patterns generated due to continuously changing local distance
110 between the coverslip and the plasma membrane are computed to derive the magnitude of local
111 tension in the membrane lower temporal fluctuations represent an increase in membrane tension
112 (Figure. 2A). After baseline imaging, Piezo1-GFP expressing Jurkat cells were subjected to sequential
113 fluorescence and IRM imaging post SDF1α addition which was followed over time. Chemokine
114 administration to Jurkat T cells led to a decrease in temporal fluctuations and an increase in
115 membrane tension when computed for the whole cellular contour (Figure 2B). The increase in
116 membrane tension was registered within few minutes after chemokine addition and gradually
117 declined over time (Figure 2C). Distribution of tension and fluctuation-amplitude in cells was also
118 affected by the action of chemokine (Supplemental figure 2A) which was accompanied by increase in
119 the membrane's degree of confinement and the effective viscosity experienced (Supplemental figure
120 2C & D). Moreover, the tension maps showed that the lamellipodial structures towards the leading
121 edges of the cells had higher tension magnitudes (Figure 2D, Supplemental figure 2B). These high-
122 tension edges are usually further emphasized at later time-points.

123 Finally, we explored if local membrane tension increase was linked to Piezo1 redistribution in the
124 chemokine-experienced T cells. Of note here, during acquisition, there is typically a time delay of 1
125 minute between measurement of tension and Piezo1-GFP fluorescence. As expected, average
126 tension peaked within the first few minutes of chemokine addition, followed by partial decline
127 (Figure 2E) as seen for the whole cell. Pixel count of Piezo1-GFP intensity showed a similar pattern,
128 albeit, at a delayed time, following the tension kinetics. In order to account for the delayed kinetics
129 of tension magnitude and Piezo1-GFP pixel count, we performed a correlation between normalised
130 Piezo1 pixel intensity at a particular time-frame, with normalised tension magnitude at the

131 preceding time frame. We observed significant positive correlation between the two parameters
132 (Figure 2F, G). Thus, IRM-coupled fluorescence microscopy revealed an increase in local membrane
133 tension in the leading edge of the moving T cells in response to chemokine receptor activation that
134 was associated with Piezo1 redistribution to the leading edges of the cells.

135

136 **Focal adhesion following chemokine receptor activation does not depend on Piezo1**

137 Focal adhesion formation is a critical step in cellular migration and activated (phosphorylated focal
138 adhesion kinases link extracellular physical cues to the cytoskeletal actomyosin scaffold (34, 35).
139 Chemokine signaling induces phosphorylation of focal adhesion kinase (FAK) and membrane
140 recruitment of the FAK complex forming focal adhesions with the extracellular substrate. FAK
141 recruits adapter proteins like paxillin to anchor with the local sub-membrane cytoskeleton made by
142 de novo F-actin polymerization. Membrane-recruited FAK complexes anchored to cytoskeleton
143 increases local membrane tension as well as recruit integrins to the membrane (36, 6, 37). This so-
144 called 'outside-in' signaling, whereby membrane recruitment of integrins (e.g.; LFA1 in T cells) is
145 initiated, is followed by integrin signaling ('inside-out' signaling) driven primarily by phosphoinositide
146 3-kinase (PI3K)-driven phosphorylation of Akt and downstream activation of Rho GTPases which in
147 turn drive extensive F-actin polymerization (38, 39). Retrograde flow of the F-actin to the rear end of
148 the moving cells, through myosin-based contractions, generates the propelling force for cells to
149 move forward following the chemokine gradient (6, 7).

150 Finding a critical role of Piezo1 in human T cell migration and a membrane tension-dependent
151 redistribution of Piezo1 to the leading edge of the moving cells led us explore if FAK recruitment to
152 the leading edge in response to chemokine stimulation was dependent on Piezo1. While
153 phosphorylated FAK (pFAK) showed striking polarity upon CCL19 stimulation on ICAM-1 beds (Figure
154 3A, B, Supplementary video 3), Piezo1 knockdown did not have any effect on pFAK polarity under
155 the same conditions (Figure 3C, D). Thus, focal adhesion formation following chemokine receptor
156 activation was not dependent on Piezo1. FAK activation recruits adapters like paxillin and vinculin
157 connecting the cortical cytoskeleton to the membrane and the extracellular matrix, thereby
158 increasing local membrane tension (34). Inhibition of FAK activation completely abrogated Piezo1
159 redistribution to the leading edge, hence the polarity (Figure 3E, F). This indicated that
160 mechanistically, FAK activation event precedes Piezo1 redistribution to the leading edge of the
161 migrating human $CD4^+$ T cells.

162

163 **Membrane recruitment of LFA1 on chemokine receptor activation disrupts with Piezo1 deficiency**

164 Integrin recruitment to the leading edge occurs downstream of FAK activation and local F-actin
165 polymerization. As expected, CCL19 stimulation led to LFA1 recruitment to the leading edge upon
166 CCL19 stimulation on ICAM1 bed (Figure 4A, B; Supplemental video 4). Moreover, Piezo1 and LFA1
167 exhibited significant colocalization upon chemokine stimulation (Figure 4C). Piezo1 downregulation
168 abrogated LFA-1 polarity (Figure 4D, E; Supplemental videos 5, 6). Thus, role of Piezo1 in
169 chemotactic migration of T cells was downstream of FAK assembly in response to chemokine
170 receptor signaling, but preceded integrins recruitment. These data together point to a mechanism
171 whereby local increase in membrane tension leading from FAK activation and assembly drives Piezo1
172 activation, which in turn is linked to LFA1 recruitment to the focal adhesions.

173 To further confirm this critical role of Piezo1 on LFA1 recruitment, we looked at the major signaling
174 event downstream of LFA1 recruitment to the leading edge, i.e., phosphorylation of Akt downstream
175 of PI3K activation, which in turn is triggered upon integrin activation. On treatment with CCL19,
176 human $CD4^+$ T cells moving on ICAM-1-coated plates did show a prominent leading-edge polarity of
177 non-phosphorylated and phosphorylated Akt (pAkt) (Figure 4F, control panel). But in Piezo1-
178 deficient cells the polarity of pAkt is abrogated (Figure 4G), not affecting the polarity of non-
179 phosphorylated AKT (Figure 4H; Supplemental videos 7, 8), substantiating the cellular signaling
180 defect due to non-recruitment of LFA1 to the leading edge membrane.

181 **Piezo1 deficiency disrupts F-actin retrograde flow in T cells despite chemokine receptor activation**

182 Piezo1-mediated sensing of membrane tension drives calcium ion influx, which in turn has been
183 shown to activate calpain and F-actin polymerization (14, 19). LFA1 recruitment is driven by local
184 actin scaffold formation following FAK assembly, which as our data indicates is perhaps contributed
185 by consolidation local actin scaffold downstream of Piezo1 activation. To confirm this, we performed
186 Ca^{2+} imaging in Piezo1-mCherry transfected Jurkat Cells using total internal reflection fluorescence
187 (TIRF) microscope in response to chemokine. We found significant colocalization of the Ca^{2+} signal
188 with the Piezo1 signal on the chemokine treated Jurkat cells (Figure 5A, B; Supplemental figure 3A,
189 B). Next to confirm that activation of calpain mediates the Piezo1 function, we observed that prior
190 inhibition with calpain inhibitor PD150606 abrogated CCL19-induced LFA1 recruitment to the leading
191 edge of the T cells (Figure 5C, D). As expected, the upstream event of pFAK polarity was not affected
192 by the calpain inhibition (Supplemental figure 3C, D).

193 While F-actin polymerization downstream of FAK is required for LFA1 recruitment, LFA1 in turn
194 drives a more robust F-actin polymerization at the leading edge, through Akt/Rho GTPase activation.

195 Leading edge F-actin undergoes retrograde flow due to myosin contractions, thereby enabling cells
196 to move forward. Thus, both at the leading edge lamellipodia and the rear edge F-actin
197 redistribution can be documented in a motile cell. We observed focal co-localization of LFA1 with F-
198 actin at the leading edge, along with a denser actin-rich protrusion in the rear edge or the uropod
199 (Figure 5C), which was abolished upon calpain inhibition (Figure 5C, E). Hence, LFA1 recruitment may
200 depend on local F-actin polarization downstream of Piezo1 activation. On the other hand, failure of
201 LFA1 recruitment and activation halts further F-actin polarization feeding the retrograde flow of
202 actin during migration.

203 Dichotomy of Piezo1 (dense leading edge distribution) and F-actin (more dense at the rear end)
204 distribution was clearly demonstrated in cells stimulated with chemokine (Figure 6A and
205 Supplemental video 9). But, no F-actin polarity was seen on downregulating Piezo1 in the T cells
206 (Figure 6B, C; Supplemental videos 10, 11). Live cell imaging of Jurkat T cells expressing Piezo1-
207 mCherry and actin-GFP on ICAM-1 coated dishes was performed in the presence or absence of
208 SDF1α (Supplemental figure 4A). Chemokine addition showed significant increase in Piezo1 polarity
209 to the front end, as shown in the earlier experiments (Figure 6E, Supplemental figure 4B, left) upon
210 chemokine stimulation when compared to untreated cells (Figure 6D, Supplemental figure 4B, left).
211 But F-actin showed a dynamic balance at both ends as expected (Figure 6E, Supplemental figure 4F,
212 right). Polar plots depicting angular distribution of Piezo1 mCherry and actin-GFP (over all time-
213 points) in the presence or absence of SDF1α are shown in Supplemental figure 4C. Representative
214 image 6F and supplemental video 12 shows Piezo1-mCherry distribution predominantly at the
215 leading edge and actin-GFP eventually accumulating at the rear end in uropod-like cellular
216 extensions in a migrating Jurkat T cell.

217 Thus, our data reveals a membrane-intrinsic event, involving a critical role of Piezo1
218 mechanosensors, within the outside-in signaling module in response to chemokine receptor
219 activation in human T cells. The mechanistic model derived from our data is depicted in Figure 7. The
220 Piezo1 mechanosensing links the focal adhesion assembly to integrins recruitment at the leading
221 edge of the human T cells migrating in response to chemokine activation and thus play a critical role
222 in chemotactic migration of human T cells.

223

224 **DISCUSSION**

225 The present study explored the role of membrane-intrinsic tension generation and the crucial role of
226 sensing this physical cue in the context of human T cell migration in response to chemokine receptor

227 activation. Deficiency of Piezo1 inhibited integrin-dependent migration, demonstrating crucial role
228 of these mechanosensors in this mode of T cell migration. As the integrin-dependent chemotactic
229 migration of T cells is a critically implicated in most patho-physiologic contexts, in the present study
230 we focused on the potential role of Piezo1 mechanosensors in this specific context.

231 Notably, a previous study in vivo in mice, using genetic deletion of Piezo1 in T cells, reported no
232 significant effect on tissue recruitment of T cells (17). Although a functional redundancy in the role
233 of Piezo1-mediated mechanosensing in mouse T cells warrants exclusion, especially in case of gene
234 deletion in developing T cells, given the considerable expression of Piezo2 as well in mouse T cells
235 (40). On the other hand, a role of Piezo1 activation in fibroblastic reticular cells in Peyer's patches
236 has been shown to regulate lymphocyte migration through tissue conduits (41). The different tissue
237 distribution of Piezo1 and Piezo2 expression in humans warranted exploring the role of Piezo1 in
238 migrating human T cells, as in humans Piezo2 is hardly expressed in the hematopoietic cells.

239 Non-invasive interference reflection microscopy allowed us to demonstrate dynamic change in
240 membrane tension at the leading edge of T cells stimulated with chemokine on ICAM1-bed which
241 was closely followed by dynamic recruitment Piezo1 locally. Chemokine receptor activation leads to
242 focal adhesion formation at the leading edge of the migrating T cells (34, 35). Our experiments
243 revealed that Piezo1 recruitment at the leading edge of the cells followed focal adhesion kinase
244 activation. Focal adhesions do increase local membrane tension as they connect the extracellular
245 environment with the cortical cytoskeleton of the cell (34). Piezo1 recruitment locally seems to be a
246 response to this membrane tension increase at focal adhesions.

247 'Outside-in' signaling downstream of focal adhesion formation recruits integrins to the leading edge
248 of the moving T cells (35, 36) which was abrogated by Piezo1 downregulation. Piezo1 has been
249 shown to drive Ca^{2+} influx into the T cells leading to calpain activation (14, 19). As expected, calpain
250 inhibition also interfered with leading edge recruitment of the integrin LFA-1. Plausibly calpain
251 activation drives local F-actin polymerization at the leading edge facilitating LFA-1 recruitment. This
252 was also supported by loss of polarity of AKT phosphorylation with Piezo1 deficiency, which is known
253 to be the major downstream signaling module that succeeds LFA-1 recruitment and activation (39,
254 42). These dysregulations in turn abrogates the retrograde flow of actin in the moving cell that is
255 essential for forward propulsion of the cell body (6, 7, 37, 41). Of note here, a role of ER-resident
256 Piezo1, in driving R-RAS-driven activation of integrins, which was again dependent on calpain
257 activation, was reported even before the mechanosensing function of Piezo1 was established (30).

258 Thus, the present study reports a hitherto unexplored role of the professional mechanosensor
259 Piezo1 in integrin dependent chemotactic movement of human T cells. In the cascade of leading
260 edge events in a moving human T cell, following chemokine receptor activation and eventually
261 leading to the retrograde flow of actin, focal adhesion formation precedes Piezo1 activation, while
262 LFA-1 recruitment is dependent on Piezo1 function.

263

264 **METHODS**

265 **Human $CD4^+$ T cell isolation and transfection.**

266 Human $CD4^+$ T lymphocytes were isolated from peripheral blood from healthy donors through
267 magnetic immunoselection. Peripheral blood samples from healthy human subjects were collected
268 on obtaining written informed consents. The studies were approved by the Human Ethics
269 Committee of CSIR-Indian Institute of Chemical Biology, India. Cells were transfected with either
270 EGFP control or Piezo1-specific siRNAs using Lonza 4D nucleofector, as per the manufacturer's
271 protocol. Briefly, cells were nucleofected in 100µl of supplemented P3 primary buffer containing
272 175ng of respective siRNAs. Nucleofection was performed using EO-115 pulse in Lonza 4D
273 nucleofector. Nucleofected cells were incubated at 37°C. 5% CO_2 in RPMI media containing 10% FBS
274 for 3 days before experiments were conducted. Knockdown was checked by qPCR measurement of
275 Piezo1 and Piezo2 transcript levels (Supplementary Figure. 1A).

276 GFP/Piezo1 siRNA co-nucleofection

277 Approximately 2×10^6 human CD4+ T lymphocytes were nucleofected with 3µg of GFP-expressing
278 plasmid along with 175ng of Piezo1-specific siRNA. Cells were incubated for 3 days before migration
279 studies.

280 Analysis of Piezo1 knockdown

281 GFP and Piezo1 siRNA co-transfected $CD4^+$ T cells were stained for Piezo1 to measure
282 downregulation. Both surface and intracellular (0.2% triton X-100 permeabilization) Piezo1 were
283 stained. Briefly, cells were collected on day and fixed in 0.5% PFA for 5 minutes on ice. Cells were
284 stained with 1.67µg/ml of rabbit anti-Piezo1 for 45 minutes at 4°C. After washing, 1.5µg/ml of anti-
285 rabbit alexa 568-IgG was added and incubated for 30 minutes at 4°C. Cells were acquired on BD LSR
286 Fortessa III after washing. Piezo1 mean fluorescence intensity (MFI) were measured both for GFP^+
287 and GFP^- cells.

288 **2-dimensional cell tracking.**

289 12-mm confocal dishes were coated with 4µg/ml of recombinant human ICAM-1 overnight at 4°C.
290 Wells were washed with 1X PBS. Tracking of GFP/Piezo1 siRNA-transfected cells were performed
291 after cell trace violet-labelling in the presence of recombinant CCL19 on ICAM1-coated dishes.
292 Stained cells were added to the wells and allowed to settle for 1 hour at 37°C. 2D tracking was
293 performed at 37°C after addition of 0.5µg/ml of recombinant human CCL19 and incubated for 10
294 minutes before acquisition. Images were acquired at regular intervals at room temperature using
295 Zeiss LSM setup at 20X magnification for a total duration of 10-15 minutes at 30 second interval.
296 $CD4^+$ T lymphocytes were RPMI without phenol red supplemented with 10% FBS and 25mM HEPES
297 during the duration of imaging.

298 **2D cell tracking analysis**

299 For tracking analyses of GFP and Piezo1 siRNA co-transfected cells, all cells above a specific threshold
300 area were used to eliminate potential debris and dead cells due to GFP plasmid transfection. Time-
301 based image stacks obtained were analysed using the Particle Tracker 2D/3D plugin of the FIJI
302 Mosaic Suite. Briefly, images were corrected for any shift in alignment during acquisition, using the
303 StackReg plugin. Corrected images were the thresholded to create a 0-255 binary mask which were
304 then used for tracking using the Particle Tracker 2D/3D plugin. Tracking provided frame-wise X-Y co-
305 ordinates of cells which were subsequently used to derive the following parameter to measure
306 motility:

307 *a. Mean-squared displacement*

308 *MSD (n)* = $\sum_{i=0}^{i=n}(x_n - x_0)^2 + (y_n - y_0)^2$ where,

309 i = 0 is the first frame,

310 i = n is the nth frame.

311 **Tranwell chemotaxis assay**

312 5µm transwell inserts were coated with 4µg/ml of recombinant human ICAM-1. Equal number of
313 primary human $CD4^+$ T cells and Jurkat cells nucleofected with control or Piezo1-specific siRNA were
314 added to the ICAM-1-coated inserts. Cells were allowed to migrate in response to recombinant
315 human CCL19 (0.5µg/ml) or SDF1α (0.1µg/ml) in the lower chamber wells for 5 hours and 1.5 hours,
316 respectively, at 37°C, 5% CO_2. Migration was halted by placing the setup on ice. Percent migration

317 was calculated by counting the number of cells in the lower chamber and dividing it by total number
318 of cells that was seeded.

319 **Overexpression of mCherry/GFP-tagged Piezo1 and Actin-GFP in Jurkat cells.**

320 GFP and mCherry-tagged Piezo1 constructs were kindly provided by Dr. Charles Cox at Victor Chang
321 Cardiac Research Laboratory, Darlinghurst, Australia. Approximately 2 million Jurkat cells were
322 nucleofected with 2-3µg of fluorescent Piezo1 construct in 100µl of supplemented SE cell line buffer.
323 Cells were pulsed using CL-120 program in Lonza 4D nucleofector. Cells were cultured in antibiotics-
324 deficient RPMI supplemented with 20% FBS for 36 hours. Overexpression was confirmed using flow
325 cytometry.

326 **Interference Reflection Microscopy and Analysis**

327 Jurkat cells were nucleofected with 2-3µg/ml of Piezo1-GFP construct. Overexpression was
328 confirmed using flow cytometry. Transfected cells were seeded on recombinant human fibronectin
329 glass-based dishes. Cells were allowed to completely adhere for 1 hour to allow IRM imaging.

330 An inverted microscope (Nikon, Japan) with 60x 1.2 NA water-immersion objective, Hg arc lamp and
331 necessary interference filter (546 ± 12 nm) were used for the interference reflection microscopy (43,
332 44) and images were captured at 19.91 frames per second using a EMCCD camera (Evolve 512 Delta;
333 Photometrics, Trenton, NJ). Cells that were significantly adhered to the glass bottom were used for
334 imaging. Regions used for analysis were stringently chosen to avoid parts farther than ~ 100 nm from
335 the coverslip – also called the first branch region (FBR) and the size chosen was 4x4 pixels
336 corresponding to ~ $(720\ nm)^2$. First, cells were imaged by IRM to take baseline reading following
337 which chemokine (SDF1α) was added. Cells were followed till 30 min with ~ 2-3 min interval post-
338 chemokine addition.

339 For stringent selection of subset of regions, extraction of parameters as well as for visualizing the
340 amplitude of fluctuations, the methodology developed previously (44, 45) was followed. 2048
341 frames corresponding to ~ 102 sec were captured and used for a single measurement of tension. The
342 analysis involved calculation of standard deviation of temporal height fluctuations (SD_{time}) and
343 estimating the power spectral density (PSD) by autoregressive technique (probability of covariance
344 or pcov) where the order is chosen to match best with PSD obtained using fast fourier transform
345 (MATLAB, Mathworks Inc., USA). For deriving mechanical parameters, the PSD is fitted with a
346 Helfrich-based model –

$$PSD(f) = \frac{4\eta_{eff} A k_B T}{\pi} \int_{q_{min}}^{q_{max}} \frac{dq}{(4\eta_{eff}(2\pi f))^2 + \left[\kappa q^3 + \sigma q + \frac{\gamma}{q}\right]^2}$$

347 with four fitting parameters (44) using fluctuation-tension (σ), effective viscosity (η_{eff}), level of
348 confinement (γ) and the effective active temperature (A)). The bending rigidity (κ) was fixed at 15
349 k_BT. Membrane fluctuation-tension closely follows membrane frame tension for a large range of
350 tension values (46). Membrane fluctuation-tension closely follows membrane frame tension for a
351 large range of tension values (46). For brevity, membrane fluctuation-tension has been referred to
352 as "tension" in the rest of the manuscript. Tension maps were created from PSDs calculated for
353 every pixel which were subsequently fitted and parameters extracted for every pixel. For analysing
354 correlation between fluorescence and tension, first the fluorescence distribution of cells was
355 plotted. Regions of intermediate intensity (around the first peak of the distribution) of a fixed
356 intensity range was filtered and the pixel count of the filtered area was plotted against the average
357 tension in those pixels. Normalization was done by diving by the maximum value in the time series.
358 Normalized pixel count, thus, reflects how area with high Piezo1-GFP at the membrane changes
359 while avoiding a small area fraction with very high Piezo1-GFP which might arise from internal
360 structures. To ensure significance of the observed differences, the statistical test undertaken was the
361 Mann-Whitney U test.

362 **Piezo1 and actin distribution in live cell imaging**

363 Jurkat cells expressing mCherry-tagged Piezo1 were seeded on ICAM-1-coated dishes. 0.1µg/ml of
364 recombinant human SDF1α was added to the cells for 15 minutes prior to imaging. Cell tracking was
365 performed in EVOS FL microscope using the PE-Texas red filter, at an interval of 1 frame per minute,
366 at room temperature. Imaging was performed for a total duration of 15 minutes.

367 For Jurkat cells transfected with Piezo1-mcherry and actin-GFP, cells were treated similarly and
368 acquired on Zeiss LSM confocal setup. Z-stack was obtained at 1µm per stack to capture the entire
369 cell. Time-lapse was imaged at an interval of 30 second per frame for a total duration of 5 minutes.
370 Confocal imaging was performed at 37°C.

371 For particle image velocimetry (PIV) analysis of Piezo1-mCherry-expressing Jurkat cells was
372 performed using the Iterative PIV plugin of FIJI. Time-lapse image stacks were split and stacks of
373 paired subsequent images were formed. Each of these stacks was then corrected for any shift in
374 alignment using the StackReg plugin. Aligned stacks were then subjected to iterative FIJI PIV analysis
375 using the conventional cross-correlation method to measure flow of fluorescent Piezo1 in

376 chemokine-treated Jurkat cells. PIV post-processing was done with default parameters and PIV
377 magnitude plots were obtained from the plugin.

378 **Measurement of cell polarity during live-cell imaging.**

379 A custom code was written in Fiji (ImageJ) to analyze the cell image time-lapse for the calculation
380 Front/Back (F/B) ratio of actin and Piezo1 expression relative to the direction of cell migration.
381 Briefly, intensity-based thresholding was performed on the actin images to create binary masks of
382 the cells. Individual cell boundaries were identified in the time-lapse, which were stored in the form
383 of polygon ROIs. The cell ROIs enabled the computation of each cell's trajectory and displacement
384 vectors from the geometrical centroid at every frame of the time-lapse video. The computation of
385 cell polarity involved fitting each cell's ROI to an ellipse and bisecting the ellipse perpendicular to the
386 migration direction. The ratio of total intensities in the leading half and the trailing half of the ellipse
387 was calculated for actin and piezo1 images to get the F/B ratio.

388 For polarity measurement of fixed confocal images, cell boundaries were similarly identified. Stored
389 ROIs were then split into two halves perpendicular to the long axis of the cell. The polarity index was
390 measured by calculating the difference of total intensities of two halves of the cell divided by the
391 sum of their total intensities. A measurement of 1 shows complete skewing of fluorescent signals to
392 one half of the cell, while a value of 0 shows uniform distribution of fluorescent signals in both cell
393 halves Representative polarity analysis Piezo1 (fixed), Piezo1 mCherry (live), pFAK (fixed),
394 CD11a/LFA-1 (fixed) and actin (fixed) of untreated and CCL19-stimulated $CD4^+$ T lymphocytes
395 (Supplemental figure 6A-F).

396 **Generation of Piezo1 mCherry and Actin-GFP polar plots.**

397 For analysis of angular/spatial distribution of Piezo1 mCherry and actin-GFP with respect to direction
398 of cell movement, cell ROIs were applied to the actin and piezo1 channels individually, to find the
399 intensity-weighted centre of mass (through all the time-points). Depending on the fluorescence
400 intensity distribution, the intensity-weighted centre of mass is shifted away from the geometric
401 centroid and towards the direction of a higher protein distribution. Thus, a vector connecting the
402 centroid (geometric centre) to the centre of mass gives the direction of polarization of the protein of
403 interest. The relative angle of the polarization vector against the cell displacement vector was
404 calculated for each frame, and a polar histogram of the angles was plotted for actin-GFP and piezo1-
405 mCherry.

406 **Fixed immunostaining for confocal imaging**

407 Untransfected human $CD4^+$ T lymphocytes were seeded on 12-mm, ICAM-1-coated glass coverslips
408 at a density of about 0.2 million cells per coverslip. Cells were incubated at 37°C, 5% CO_2 for 1.5
409 hours. 0.5µg/ml of recombinant human CCL19 was added to each coverslip and incubated for 20-30
410 minutes at 37°C. Post-treatment, cells were fixed in 4% paraformaldehyde for 15 minutes at room
411 temperature. Blocking was performed in 3% bovine serum albumin in 1X PBS containing 0.2% Triton
412 X-100 for 50 minutes at room temperature. Primary rabbit anti-human Piezo1 (Proteintech) was
413 added at a dilution of 1:100 (5µg/ml) and incubated at room temperature for 1 to 1.5 hours. Alexa
414 568-conjugated anti-rabbit IgG was added at a dilution of 1:350 (5.7µg/ml), and incubated for
415 further 45-50 minutes. Nuclear staining was performed for 1 minute with Hoechst 33342 dye at a
416 concentration of 1µg/ml in 1X PBS. All washes between steps were carried out in 1X PBS. Stained
417 cells were then mounted on Vectashield® mounting media and sealed before confocal imaging. For
418 Piezo1 and CD44 co-staining, rabbit anti-Piezo1 and mouse anti-human CD44 were used at a
419 concentration of 5µg/ml, each. Alexa 488-conjugated anti-rabbit IgG and alexa 633-conjugated anti-
420 mouse IgG were used at a concentration of 5.7µg/ml, each.

421 For actin imaging, LifeAct-TagGFP2 protein was added at a concentration of 0.5µg/ml, and incubated
422 for 45 minutes at room temperature before washing. For LFA-1 ($\alpha_L\beta2$) staining, mouse anti-human
423 CD11a (α_L subunit) was added at a concentration of 5µg/ml, followed by addition of anti-mouse
424 Alexa 594-conjugated IgG. For LFA-1 and Piezo1 co-staining, primary antibodies were added at above
425 concentrations, with Alexa 568-conjugated anti-rabbit IgG (for Piezo1) and Alexa 488-conjuagted
426 anti-mouse IgG (for CD11a/LFA-1). Rabbit/mouse anti-phosphorylated FAK (Tyr-397) was used to
427 stain pFAK to detect focal adhesions. These cells were treated with chemokine CCL19 for 10 minutes
428 prior to fixation. While doing confocal microscopy, Z-stacks were captured at 0.5µm intervals.
429 Confocal images are represented are maximum intensity projections of the Z-slices.
430 3Dprojectionfunction of Fiji was used to create a 3D rendering of the Z-slices, using the brightest
431 point method of projection.

432 **TIRF Imaging and Ca^{2+}-Piezo1 colocalization**

433 Ca^{2+}-Piezo1 imaging involved incubating cells with Fluo-3 AM (2.5 µM) in HBSS buffer for 30 minutes
434 at 37˚C, followed by washing and imaging in RPMI containing 10% FBS, and 25 mM HEPES media.
435 Jurkat cell were transfected with Piezo1 mCherry plasmid and only those expressing Piezo1 mCherry
436 were selected for the study. Dual-colour sequential TIRF imaging was employed, with Piezo1
437 mCherry being imaged at 300 ms (100 frames) and Ca2+ imaging performed using a 10 ms exposure
438 time (2000 frames). The short exposure for Ca2+ was used to capture transient local peaks of
439 fluorescence which would otherwise average out at longer exposure times. The maximum projection

440 of the time series was used to detect local peaks using adaptive local thresholding (MATLAB), and a
441 size filter was used to exclude large objects identified with a relatively low Ca^{2+} gradient. For each
442 specific set of settings, the Ca^{2+} signal objects detected were used to calculate the average cluster
443 size and total area of objects. Uniform random numbers were used to simulate clusters with
444 appropriate probability to ensure that the final area of the simulated Ca^{2+} clusters closely matched
445 the real data. The overlap between the real Ca^{2+} signal and Piezo1 objects was compared with the
446 simulated data to test for deviation from a random placement of Ca^{2+} spots. To assess the
447 robustness of the results, different combinations of size filters of Piezo1 and Ca^{2+} objects were used,
448 ranging from 50 to 350 pixels.

449 **Calpain Inhibition**

450 PD150606 (Merck, India), a non-competitive calpain 1 and 2 inhibitors, was used at a concentration
451 of 100µM. Untransfected $CD4^+$ T lymphocytes were treated with PD150606 for 1 hour at 37°C prior
452 to treatment of chemokine. Post -chemokine treatment cells were stained either with pFAK as
453 described.

454 **Focal adhesion kinase Inhibition**

455 FAK inhibitor 14 (1,2,4,5-Benzenetetraamine tetrahydrochloride) was used to selectively inhibit FAK
456 activity. Inhibitor was added at a final concentration 10µM, 1 hour prior to treatment with
457 recombinant CCL19. Post-treatment with CCL19, $CD4^+$ T lymphocytes were stained with Piezo1 for
458 confocal imaging.

459 **Piezo1 Inhibition**

460 Primary human $CD4^+$ T cells were incubated with 10µM of GsMTx4 for 1 hour prior to transwell
461 chemotaxis assay in response to recombinant CCL19.

462 **Statistics**

463 Student t-test was used to calculate significance.

464

465 **ACKNOWLEDGEMENTS**

466 The study was funded by Council of Scientific and Industrial Research, India (Grant no. FBR MLP-
467 140). D.G. is a recipient of Swarnajayanti Fellowship from Department of Science and Technology,

468 Government of India. The authors express their gratitude for provision of the Piezo1 constructs by
469 Dr. Charles Cox, Victor Chang Institute of Cardiac Research, Australia.

470 The authors declare no competing interests

471 C.S.C.L. designed, performed and analyzed most of the experiments, prepared the figures and took
472 part in writing the manuscript; T.M., B.S. and C.S.C.L. performed the IRM experiments; T.M. and B.S.
473 analyzed IRM data; C.S.C.L., P.B. and D.K.S. performed image analyses; Pu.B., M.A.H., B.P.S., J.S. and
474 R.D. helped with cell culture and confocal microscopy experiments; D.G. conceptualized and
475 supervised the study, acquired funding, designed experiments and wrote the manuscript with input
476 from all authors.

477

478 **REFERENCES**

479 1. Shechter R, London A, Schwartz M. Orchestrated leukocyte recruitment to immune-
480 privileged sites: absolute barriers versus educational gates. Nat Rev Immunol. 2013
481 Mar;13(3):206-18. doi: 10.1038/nri3391.
482 2. Krummel MF, Bartumeus F, Gérard A. T cell migration, search strategies and mechanisms.
483 Nat Rev Immunol. 2016 Mar;16(3):193-201. doi: 10.1038/nri.2015.16.
484 3. Woodland DL, Kohlmeier JE. Migration, maintenance and recall of memory T cells in
485 peripheral tissues. Nat Rev Immunol. 2009 Mar;9(3):153-61. doi: 10.1038/nri2496.
486 4. Masopust D, Schenkel JM. The integration of T cell migration, differentiation and function.
487 Nat Rev Immunol. 2013 May;13(5):309-20. doi: 10.1038/nri3442.
488 5. Fowell DJ, Kim M. The spatio-temporal control of effector T cell migration. Nat Rev Immunol.
489 2021 Sep;21(9):582-596. doi: 10.1038/s41577-021-00507-0.
490 6. Dupré L, Houmadi R, Tang C, Rey-Barroso J. T Lymphocyte Migration: An Action Movie
491 Starring the Actin and Associated Actors. Front Immunol. 2015 Nov 18;6:586. doi:
492 10.3389/fimmu.2015.00586.
493 7. Nordenfelt P, Moore TI, Mehta SB, Kalappurakkal JM, Swaminathan V, Koga N, Lambert TJ,
494 Baker D, Waters JC, Oldenbourg R, Tani T, Mayor S, Waterman CM, Springer TA. Direction of
495 actin flow dictates integrin LFA-1 orientation during leukocyte migration. Nat Commun. 2017
496 Dec 11;8(1):2047. doi: 10.1038/s41467-017-01848-y.
497 8. Moreau HD, Piel M, Voituriez R, Lennon-Duménil AM. Integrating Physical and Molecular
498 Insights on Immune Cell Migration. Trends Immunol. 2018 Aug;39(8):632-643. doi:
499 10.1016/j.it.2018.04.007.

500 9. Shannon MJ, Pineau J, Griffié J, Aaron J, Peel T, Williamson DJ, Zamoyska R, Cope AP, Cornish
501 GH, Owen DM. Differential nanoscale organisation of LFA-1 modulates T-cell migration. J Cell
502 Sci. 2019 Oct 16;133(5):jcs232991. doi: 10.1242/jcs.232991.
503 10. Coste B, Mathur J, Schmidt M, Earley TJ, Ranade S, Petrus MJ, Dubin AE, Patapoutian A.
504 Piezo1 and Piezo2 are essential components of distinct mechanically activated cation
505 channels. Science. 2010 Oct 1;330(6000):55-60. doi: 10.1126/science.1193270.
506 11. Coste B, Xiao B, Santos JS, Syeda R, Grandl J, Spencer KS, Kim SE, Schmidt M, Mathur J, Dubin
507 AE, Montal M, Patapoutian A. Piezo proteins are pore-forming subunits of mechanically
508 activated channels. Nature. 2012 Feb 19;483(7388):176-81. doi: 10.1038/nature10812.
509 12. Syeda R, Florendo MN, Cox CD, Kefauver JM, Santos JS, Martinac B, Patapoutian A. Piezo1
510 Channels Are Inherently Mechanosensitive. Cell Rep. 2016 Nov 8;17(7):1739-1746. doi:
511 10.1016/j.celrep.2016.10.033.
512 13. Murthy SE, Dubin AE, Patapoutian A. Piezos thrive under pressure: mechanically activated
513 ion channels in health and disease. Nat Rev Mol Cell Biol. 2017 Dec;18(12):771-783. doi:
514 10.1038/nrm.2017.92. Epub 2017 Oct 4. PMID: 28974772.
515 14. Liu CSC, Raychaudhuri D, Paul B, Chakrabarty Y, Ghosh AR, Rahaman O, Talukdar A, Ganguly
516 D. Cutting Edge: Piezo1 Mechanosensors Optimize Human T Cell Activation. J Immunol. 2018
517 Feb 15;200(4):1255-1260. doi: 10.4049/jimmunol.1701118.
518 15. Atcha H, Jairaman A, Holt JR, Meli VS, Nagalla RR, Veerasubramanian PK, Brumm KT, Lim HE,
519 Othy S, Cahalan MD, Pathak MM, Liu WF. Mechanically activated ion channel Piezo1
520 modulates macrophage polarization and stiffness sensing. Nat Commun. 2021 May
521 31;12(1):3256. doi: 10.1038/s41467-021-23482-5.
522 16. Geng J, Shi Y, Zhang J, Yang B, Wang P, Yuan W, Zhao H, Li J, Qin F, Hong L, Xie C, Deng X, Sun
523 Y, Wu C, Chen L, Zhou D. TLR4 signalling via Piezo1 engages and enhances the macrophage
524 mediated host response during bacterial infection. Nat Commun. 2021 Jun 10;12(1):3519.
525 doi: 10.1038/s41467-021-23683-y.
526 17. Jairaman A, Othy S, Dynes JL, Yeromin AV, Zavala A, Greenberg ML, Nourse JL, Holt JR,
527 Cahalan SM, Marangoni F, Parker I, Pathak MM, Cahalan MD. Piezo1 channels restrain
528 regulatory T cells but are dispensable for effector CD4+ T cell responses. Sci Adv. 2021 Jul
529 7;7(28):eabg5859. doi: 10.1126/sciadv.abg5859.
530 **18.** Jäntti H, Sitnikova V, Ishchenko Y, Shakirzyanova A, Giudice L, Ugidos IF, Gómez-Budia M,
531 Korvenlaita N, Ohtonen S, Belaya I, Fazaludeen F, Mikhailov N, Gotkiewicz M, Ketola K,
532 Lehtonen Š, Koistinaho J, Kanninen KM, Hernández D, Pébay A, Giugno R, Korhonen P,

533 Giniatullin R, Malm T. Microglial amyloid beta clearance is driven by PIEZO1 channels. J
534 Neuroinflammation. 2022 Jun 15;19(1):147. doi: 10.1186/s12974-022-02486-y.
535 19. Liu CSC, Ganguly D. Mechanical Cues for T Cell Activation: Role of Piezo1 Mechanosensors.
536 Crit Rev Immunol. 2019;39(1):15-38. doi: 10.1615/CritRevImmunol.2019029595.
537 20. Ma S, Dubin AE, Zhang Y, Mousavi SAR, Wang Y, Coombs AM, Loud M, Andolfo I,
538 Patapoutian A. A role of PIEZO1 in iron metabolism in mice and humans. Cell. 2021 Feb
539 18;184(4):969-982.e13. doi: 10.1016/j.cell.2021.01.024.
540 21. He Y, Deng B, Liu S, Luo S, Ning Y, Pan X, Wan R, Chen Y, Zhang Z, Jiang J, Xu H, Xia M, Li J.
541 Myeloid Piezo1 Deletion Protects Renal Fibrosis by Restraining Macrophage Infiltration and
542 Activation. Hypertension. 2022 May;79(5):918-931. doi:
543 10.1161/HYPERTENSIONAHA.121.18750.
544 22. Huang Z, Sun Z, Zhang X, Niu K, Wang Y, Zheng J, Li H, Liu Y. Loss of stretch-activated
545 channels, PIEZOs, accelerates non-small cell lung cancer progression and cell migration.
546 Biosci Rep. 2019 Mar 22;39(3): BSR20181679. doi: 10.1042/BSR20181679.
547 23. Chubinskiy-Nadezhdin VI, Vasileva VY, Vassilieva IO, Sudarikova AV, Morachevskaya EA,
548 Negulyaev YA. Agonist-induced Piezo1 activation suppresses migration of transformed
549 fibroblasts. Biochem Biophys Res Commun. 2019 Jun 18;514(1):173-179. doi:
550 10.1016/j.bbrc.2019.04.139.
551 24. Mousawi F, Peng H, Li J, Ponnambalam S, Roger S, Zhao H, Yang X, Jiang LH. Chemical
552 activation of the Piezo1 channel drives mesenchymal stem cell migration via inducing ATP
553 release and activation of P2 receptor purinergic signaling. Stem Cells. 2020 Mar;38(3):410-
554 421. doi: 10.1002/stem.3114.
555 25. Wang X, Cheng G, Miao Y, Qiu F, Bai L, Gao Z, Huang Y, Dong L, Niu X, Wang X, Li Y, Tang H,
556 Xu Y, Song X. Piezo type mechanosensitive ion channel component 1 facilitates gastric
557 cancer omentum metastasis. J Cell Mol Med. 2021 Feb;25(4):2238-2253. doi:
558 10.1111/jcmm.16217.
559 26. Gao L, Ji Y, Wang L, He M, Yang X, Qiu Y, Sun X, Ji Z, Yang G, Zhang J, Li S, Dai L, Zhang L.
560 Suppression of Esophageal Squamous Cell Carcinoma Development by Mechanosensitive
561 Protein Piezo1 Downregulation. ACS Omega. 2021 Apr 12;6(15):10196-10206. doi:
562 10.1021/acsomega.1c00505.
563 27. Holt JR, Zeng WZ, Evans EL, Woo SH, Ma S, Abuwarda H, Loud M, Patapoutian A, Pathak MM.
564 Spatiotemporal dynamics of PIEZO1 localization controls keratinocyte migration during
565 wound healing. Elife. 2021 Sep 27;10:e65415. doi: 10.7554/eLife.65415.

566 28. Velasco-Estevez M, Koch N, Klejbor I, Caratis F, Rutkowska A. Mechanoreceptor Piezo1 Is
567 Downregulated in Multiple Sclerosis Brain and Is Involved in the Maturation and Migration
568 of Oligodendrocytes in vitro. Front Cell Neurosci. 2022 May 26;16:914985. doi:
569 10.3389/fncel.2022.914985.
570 29. Hung WC, Yang JR, Yankaskas CL, Wong BS, Wu PH, Pardo-Pastor C, Serra SA, Chiang MJ, Gu
571 Z, Wirtz D, Valverde MA, Yang JT, Zhang J, Konstantopoulos K. Confinement Sensing and
572 Signal Optimization via Piezo1/PKA and Myosin II Pathways. Cell Rep. 2016 May
573 17;15(7):1430-1441. doi: 10.1016/j.celrep.2016.04.035.
574 30. McHugh BJ, Buttery R, Lad Y, Banks S, Haslett C, Sethi T. Integrin activation by Fam38A uses a
575 novel mechanism of R-Ras targeting to the endoplasmic reticulum. J Cell Sci. 2010 Jan
576 1;123(Pt 1):51-61. doi: 10.1242/jcs.056424.
577 31. Xiao B. 2020. Levering Mechanically Activated Piezo Channels for Potential Pharmacological
578 Intervention. Annu Rev PharmacolToxicol. 60:195-218. doi: 10.1146/annurev-pharmtox-
579 010919-023703.
580 32. Barr VA, Bunnell SC. Interference reflection microscopy. Curr Protoc Cell Biol. 2009 Dec;
581 Chapter 4: Unit 4.23. doi: 10.1002/0471143030.cb0423s45.
582 33. Chakraborty M, Mukherjee B, Nalinakshan N, Biswas A, Nayak RK, Sinha B. Effect of
583 heterogeneous substrate adhesivity of follower cells on speed and tension profile of leader
584 cells in primary keratocyte collective cell migration. Biol Open. 2022 Mar
585 15;11(3):bio058893. doi: 10.1242/bio.058893.
586 34. Mitra SK, Hanson DA, Schlaepfer DD. Focal adhesion kinase: in command and control of cell
587 motility. Nat Rev Mol Cell Biol. 2005 Jan;6(1):56-68. doi: 10.1038/nrm1549.
588 35. Katoh K. FAK-Dependent Cell Motility and Cell Elongation. Cells. 2020 Jan 12;9(1):192. doi:
589 10.3390/cells9010192.
590 36. Yamashiro S, Watanabe N. A new link between the retrograde actin flow and focal
591 adhesions. J Biochem. 2014 Nov;156(5):239-48. doi: 10.1093/jb/mvu053.
592 37. Martino F, Perestrelo AR, Vinarský V, Pagliari S, Forte G. Cellular Mechanotransduction:
593 From Tension to Function. Front Physiol. 2018 Jul 5;9:824. doi: 10.3389/fphys.2018.00824.
594 38. Sánchez-Martín L, Sánchez-Sánchez N, Gutiérrez-López MD, Rojo AI, Vicente-Manzanares M,
595 Pérez-Alvarez MJ, Sánchez-Mateos P, Bustelo XR, Cuadrado A, Sánchez-Madrid F, Rodríguez-
596 Fernández JL, Cabañas C. Signaling through the leukocyte integrin LFA-1 in T cells induces a
597 transient activation of Rac-1 that is regulated by Vav and PI3K/Akt-1. J Biol Chem. 2004 Apr
598 16;279(16):16194-205. doi: 10.1074/jbc.M400905200.

599 39. Roy NH, Kim SHJ, Buffone A Jr, Blumenthal D, Huang B, Agarwal S, Schwartzberg PL, Hammer
600 DA, Burkhardt JK. LFA-1 signals to promote actin polymerization and upstream migration in T
601 cells. J Cell Sci. 2020 Sep 9;133(17):jcs248328. doi: 10.1242/jcs.248328.
602 40. Ganguly D. Can Piezo2 substitute Piezo1 function in the context of T cell-specific deletion in
603 mice? Sci Adv, e-Letter published Sep 8, 2021, in response to Jairaman A et al.,
604 41. Chang JE, Buechler MB, Gressier E, Turley SJ, Carroll MC. Mechanosensing by Peyer's patch
605 stroma regulates lymphocyte migration and mucosal antibody responses. Nat Immunol.
606 2019 Nov;20(11):1506-1516. doi: 10.1038/s41590-019-0505-z.
607 42. Roy NH, MacKay JL, Robertson TF, Hammer DA, Burkhardt JK. Crk adaptor proteins mediate
608 actin-dependent T cell migration and mechanosensing induced by the integrin LFA-1. Sci
609 Signal. 2018 Dec 11;11(560):eaat3178. doi: 10.1126/scisignal.aat3178.
610 43. Limozin L, Sengupta K. Quantitative reflection interference contrast microscopy (RICM) in
611 soft matter and cell adhesion. Chemphyschem. 2009 Nov 9;10(16):2752-68.
612 44. Biswas A, Alex A, Sinha B. Mapping Cell Membrane Fluctuations Reveals Their Active
613 Regulation and Transient Heterogeneities. Biophys J. 2017 Oct 17;113(8):1768-1781. doi:
614 10.1016/j.bpj.2017.08.041.
615 45. Biswas A, Kashyap P, Datta S, Sengupta T, Sinha B. Cholesterol Depletion by MβCD Enhances
616 Cell Membrane Tension and Its Variations-Reducing Integrity. Biophys J. 2019 Apr
617 23;116(8):1456-1468.
618 46. Shiba H, Noguchi H, Fournier JB. Monte Carlo study of the frame, fluctuation and internal
619 tensions of fluctuating membranes with fixed area. Soft Matter. 2016 Feb 28;12(8):2373-80.
620 doi: 10.1039/c5sm01900a.

621

622

623 **FIGURE LEGENDS**

624

625 **Figure 1. Piezo1 deficiency abrogates integrin-dependent motility in human T cells which is**
626 **mediated through redistribution of Piezo1 at the leading edge in response to chemokine**
627 **stimulation.**

628 **A.** MSD versus time calculated for GFP^+ (potential Piezo1-knockdown cells) and GFP^- (potential
629 control cells) in GFP plasmid and Piezo1 siRNA co-transfected human $CD4^+$ T lymphocytes, that were
630 allowed to migrate in presence of recombinant CCL19 on ICAM1-coated dishes. **B.** Representative
631 tracks of GFP^+ and GFP^- $CD4^+$ T lymphocytes. Comparisons of **C.** % GFP^+ cells after 72 hours of
632 nucleofection **D & E.** 3D transwell migration assay of siRNA-transfected primary human $CD4^+$ T
633 lymphocytes (D) and Jurkat T cells (E), respectively. Data representative of at least 3 independent
634 experiments. **F.** Representative confocal images of Piezo1 distribution in fixed untreated and CCL19-
635 treated $CD4^+$ T lymphocytes. 63X oil magnification. **G.** Comparison between Piezo1 polarity index
636 calculated for fixed, stained, human $CD4^+$ T lymphocytes with or without 0.5µg/ml CCL19 treatment
637 for 20-30 minutes. n > 510 random cells, each. **H.** Piezo1 polarity index calculated for Jurkat cells,
638 expressing mCherry-tagged Piezo1 during live-cell tracking in the presence of recombinant SDF1α.
639 Each dot represents polarity index of each cell, averaged over all the time-frames. **I.** Representative
640 time kinetics of particle image velocimetry (PIV) analysis of Piezo1-mcherry transfected Jurkat cells,
641 allowed to move on ICAM-coated dishes in the presence of recombinant SDF1α. Top panel: No
642 chemokine. Bottom Panel: SDF1α.

643

644 **Figure 2. Piezo1 redistribution in migrating T cells follow increased membrane tension in the**
645 **leading edge**

646 **A.** Schematic illustration of interference reflection microscopy imaging setup. **B.** Probability
647 distribution of amplitude of temporal fluctuations (SD_{time}, left) and tension (right) before and after
648 addition of chemokines. **C.** Temporal trajectory of tension of cells before and after addition of
649 chemokine with ** indicating significant difference from control. **D.** Representative IRM images of
650 Jurkat cells (top), corresponding tension maps (middle) and R^2 maps (bottom), before and after
651 chemokine treatment. **E** Correlation between normalized Piezo intensity, tension magnitudes with
652 time. **F.** Scatter plot to show correlation between normalized pixel count of Piezo1 and normalized
653 tension. Piezo1 intensity at specific time-points were correlated with tension magnitudes at the
654 preceding timepoints. Normalization has been done such that the maximum value is set to 1 and

655 others are accordingly scaled. **G.** Colour-coded Piezo1-GFP intensity map (left), epifluorescence
656 image (middle), and tension map (right) of representative Piezo1-GFP expressing Jurkat cell, after 30
657 minutes of 0.1μg/ml of SDF1α treatment.

658

659 **Figure 3. Focal adhesion following chemokine receptor activation does not depend on Piezo1**

660 **A.** Representative confocal images of human $CD4^+$ T lymphocytes, fixed and stained for phospho-FAK
661 (pFAK) under untreated and CCL19-treated conditions. **B.** Increased polarity of pFAK upon
662 chemokine stimulation of $CD4^+$ T lymphocytes as compared to unstimulated controls. N > 120 cells,
663 each. **C.** Representative confocal images of pFAK distribution in control and Piezo1 siRNA-transfected
664 $CD4^+$ T lymphocytes stimulated with chemokine. **D**. Comparison of pFAK polarity in CCL19-stimulated
665 control and Piezo1-knockdown $CD4^+$ T lymphocytes. n > 450 random cells, each. **E.** Representative
666 confocal images of stained Piezo1 in $CD4^+$ T cells stimulated with CCL19 in the presence or absence
667 of FAK inhibitor 14. **F.** Effect of FAK inhibition on Piezo1 polarity in $CD4^+$ T lymphocytes stimulated
668 with recombinant CCL19 versus untreated cells. n > 600 random cells, each. Data represented from
669 at least 3 independent experiments.

670

671 **Figure 4. Membrane recruitment of LFA1 on chemokine receptor activation disrupts with Piezo1**
672 **deficiency.**

673 **A.** Representative confocal images of fixed, immunostained Piezo1 and LFA1 in unstimulated and
674 CCL19-stimulated $CD4^+$ T lymphocytes. **B.** Increased LFA1 polarity in response to recombinant CCL19
675 stimulation in $CD4^+$ T cells. n > 295 random cells, each. **C.** Manders' co-localisation analysis of Piezo1
676 and LFA1 in untreated and CCL19-treated $CD4^+$ T lymphocytes. **D.** Comparison of LFA1 polarity in
677 chemokine-treated control and Piezo1 knockdown $CD4^+$ T lymphocytes. **E.** Representative confocal
678 stained images of LFA1 polarity of CCL19-treated control and Piezo1-knockdown $CD4^+$ T
679 lymphocytes. n > 490 random cells, each. **F.** Representative confocal images of phospho-Akt (pAkt)
680 and Akt distribution upon chemokine treatment of control and Piezo1-knockdown cells. **G & H.**
681 Quantitative analyses of pAkt (M) and Akt (N) polarity in control and Piezo1-knockdown cells after
682 CCL19-treatment. n > 580 random cells, each. Data represented from at least 3 independent
683 experiments.

684

685

686

687 **Figure 5. Local Ca^{2+} mobilization with Piezo1 redistribution upon chemokine stimulation.**

688 **A.** Representative TIRF image of a Jurkat Cell stained with Fluo3AM and transiently expressing with
689 Piezo1 mCherry. Lower panel: zoomed in image and overlap of binary images of objects detected
690 from Calcium and Piezo channels as well as simulated randomly placed punctas having similar total
691 (in the zoomed in section) and average area as that of the Calcium punctas detected in the real
692 images. Overlap RGB image shows the overlap between Real Calcium (Red) and piezo puncta
693 (Green), overlap puncta (Yellow), simulated calcium puncta (blue). **B.** Comparison between
694 percentage calcium colocalization of simulated data and real data. * Denote p value < 0.05
695 calculated using Mann Whitney U test. N cell= 52 (13 cells x 4 time points). NROIS= 52. **C.**
696 Representative confocal images of LFA1 and actin distribution in CCL19-stimulated CD4+ T
697 lymphocytes with or without inhibition of calpain. 100µM of PD15606 was added to the cells 1 hour
698 prior to addition of chemokine. Quantitative comparisons of **D.** LFA1 and **E.** actin polarity upon
699 chemokine stimulation, in the presence or absence of calpain pre-inhibition. N > 290 random cells,
700 each.

701

702 **Figure 6. Piezo1 deficiency disrupts F-actin retrograde flow in T cells despite chemokine receptor**
703 **activation.**

704 **A.** Representative fixed confocal images of actin and Piezo1 distribution in $CD4^+$ T lymphocytes after
705 30 mins of 0.5µg/ml recombinant CCL19 treatment. **B.** Quantitative comparison of actin polarity in
706 control and Piezo1-knockdown $CD4^+$ T lymphocytes cells after 30 mins of chemokine treatment. n >
707 300 random cells, each. **C.** Representative fixed confocal images of actin distribution in chemokine-
708 treated, control and Piezo1-knockdown $CD4^+$ T lymphocytes. Front-back (F/B) of Piezo1 and actin-
709 GFP in SDF1α treated **(D)** and untreated **(E)** Jurkat cells co-expressing actin-GFP and Piezo1-mCherry.
710 **F.** A snapshot of time-lapse imaging of Piezo1-mCherry and actin-GFP expressing Jurkat cell treated
711 with 0.1µg/ml of SDF1α. Image is maximum Z-projection of the cell at 63X/1.40 magnification.

712

713 **Figure 7. The mechanistic model depicting involvement of Piezo1 mechanosensing in leading edge**
714 **events in a migrating T cell.**

715 Proposed model suggests chemokine receptor activation in human T cells lead to focal adhesion
716 kinase activation and focal adhesion formation. Focal adhesions lead to localized increase in

717 membrane tension at the leading edge plasma membrane which leads to Piezo1 recruitment and
718 activation. Piezo1 activation leads to calpain activation which potentially drives further cytoskeletal
719 consolidation to recruit integrin LFA1. LFA1 recruitment and activation lead to phosphorylation of
720 AKT and downstream signaling eventually driving the retrograde actin flow in migrating human T
721 cells.

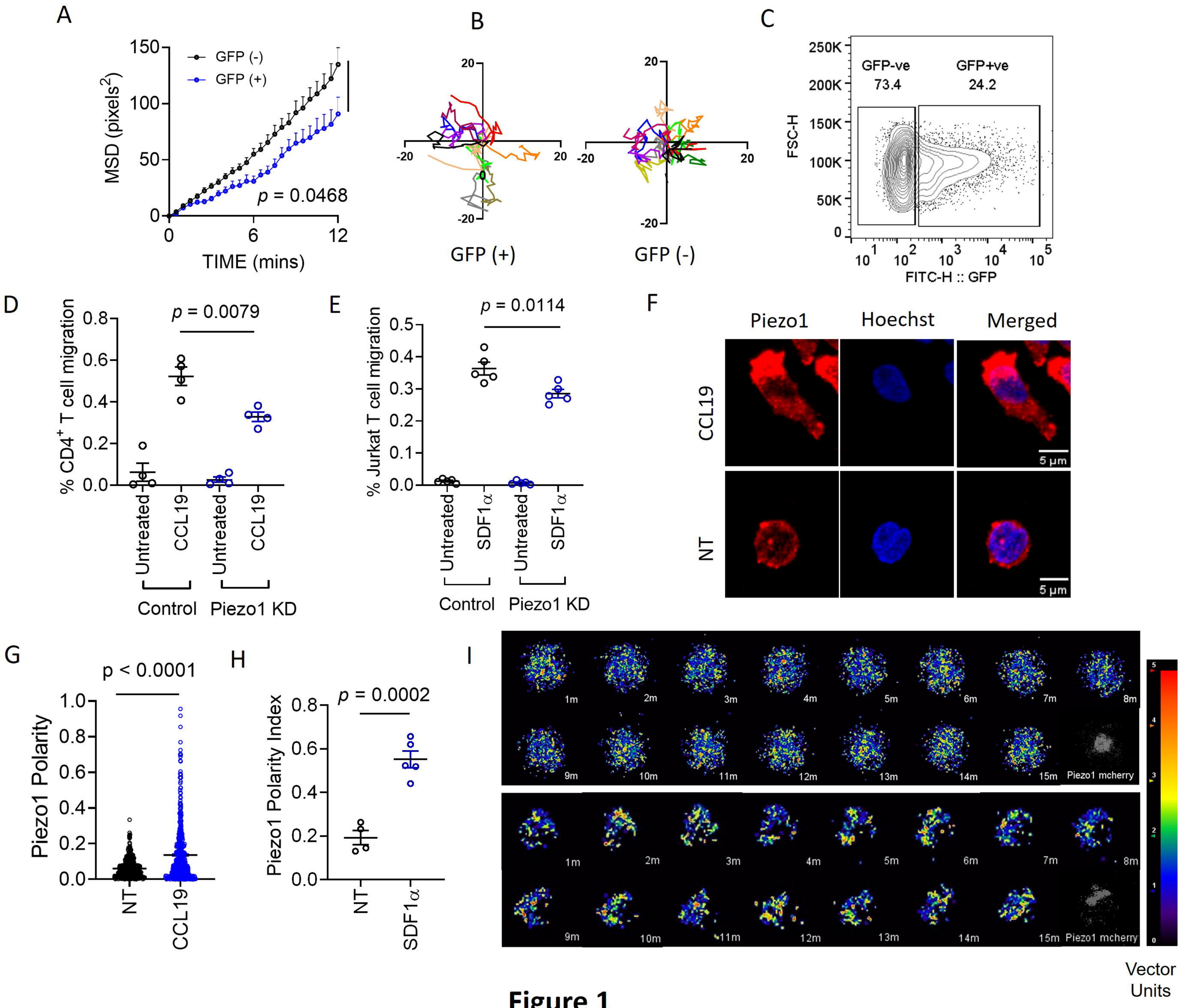
A
MSD (pixels²)
GFP (-)
GFP (+)
p = 0.0468
TIME (mins)
B
GFP (+)
GFP (-)
C
GFP-ve
73.4
GFP+ve
24.2
FSC-H
FITC-H :: GFP
D
% CD4⁺ T cell migration
p = 0.0079
Untreated
CCL19
Control
Piezo1 KD
E
% Jurkat T cell migration
p = 0.0114
Untreated
SDF1α
Control
Piezo1 KD
F
Piezo1
Hoechst
Merged
CCL19
NT
5 µm
G
Piezo1 Polarity
p < 0.0001
NT
CCL19
H
Piezo1 Polarity Index
p = 0.0002
NT
SDF1α
I
1m
2m
3m
4m
5m
6m
7m
8m
9m
10m
11m
12m
13m
14m
15m
Piezo1 mcherry
Vector Units

Figure 1

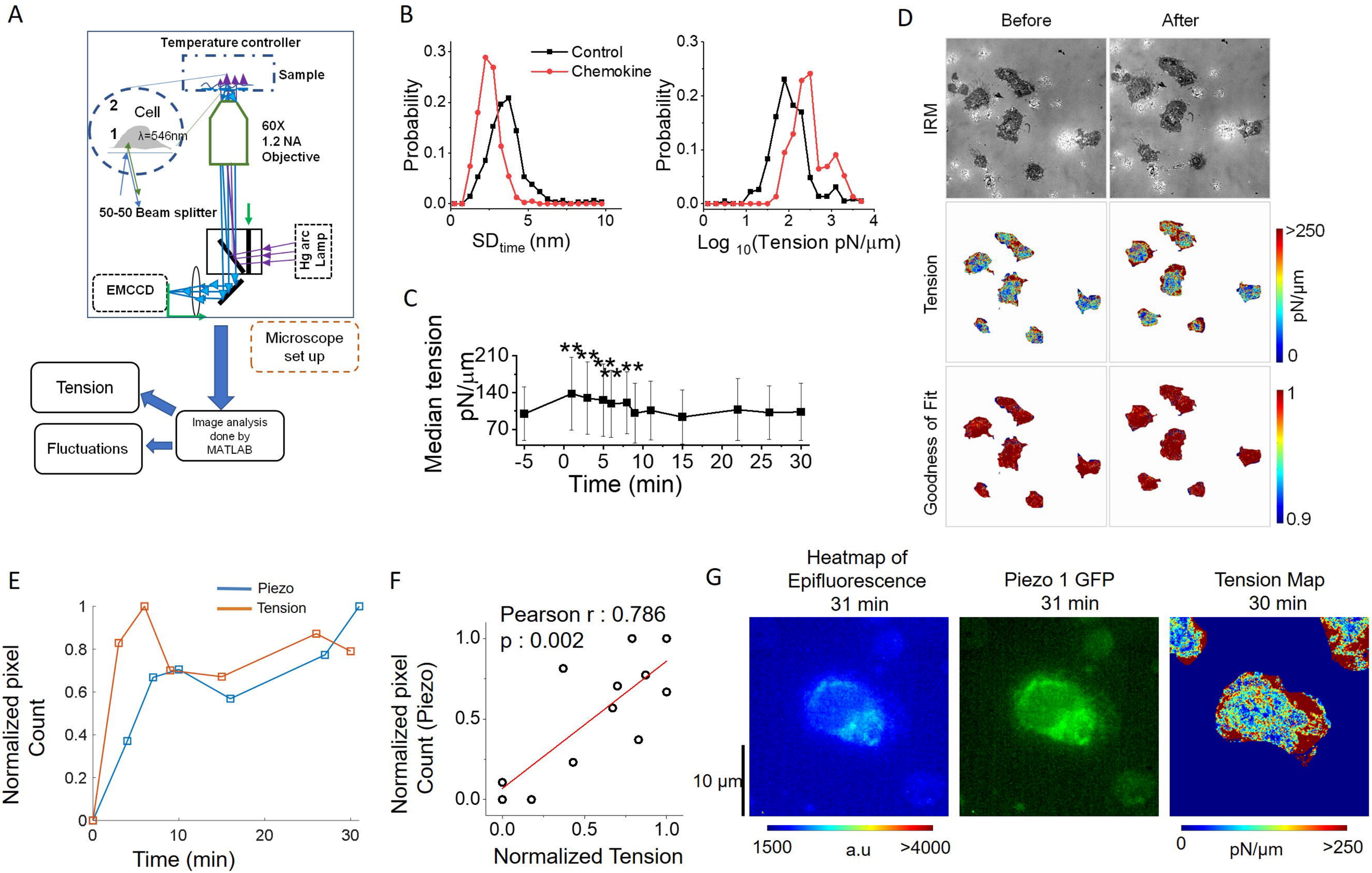
A
Temperature controller
Sample
Cell
2
1
λ=546nm
60X
1.2 NA
Objective
50-50 Beam splitter
Hg arc Lamp
EMCCD
Microscope set up
Tension
Fluctuations
Image analysis done by MATLAB
B
Control
Chemokine
Probability
SD time (nm)
Log 10(Tension pN/μm)
C
Median tension pN/μm
Time (min)
D
Before
After
IRM
Tension
Goodness of Fit
>250
pN/μm
0
1
0.9
E
Piezo
Tension
Normalized pixel Count
Time (min)
F
Pearson r : 0.786
p : 0.002
Normalized pixel Count (Piezo)
Normalized Tension
G
Heatmap of Epifluorescence 31 min
Piezo 1 GFP 31 min
Tension Map 30 min
10 μm
1500
a.u
>4000
0
pN/μm
>250

Figure 2

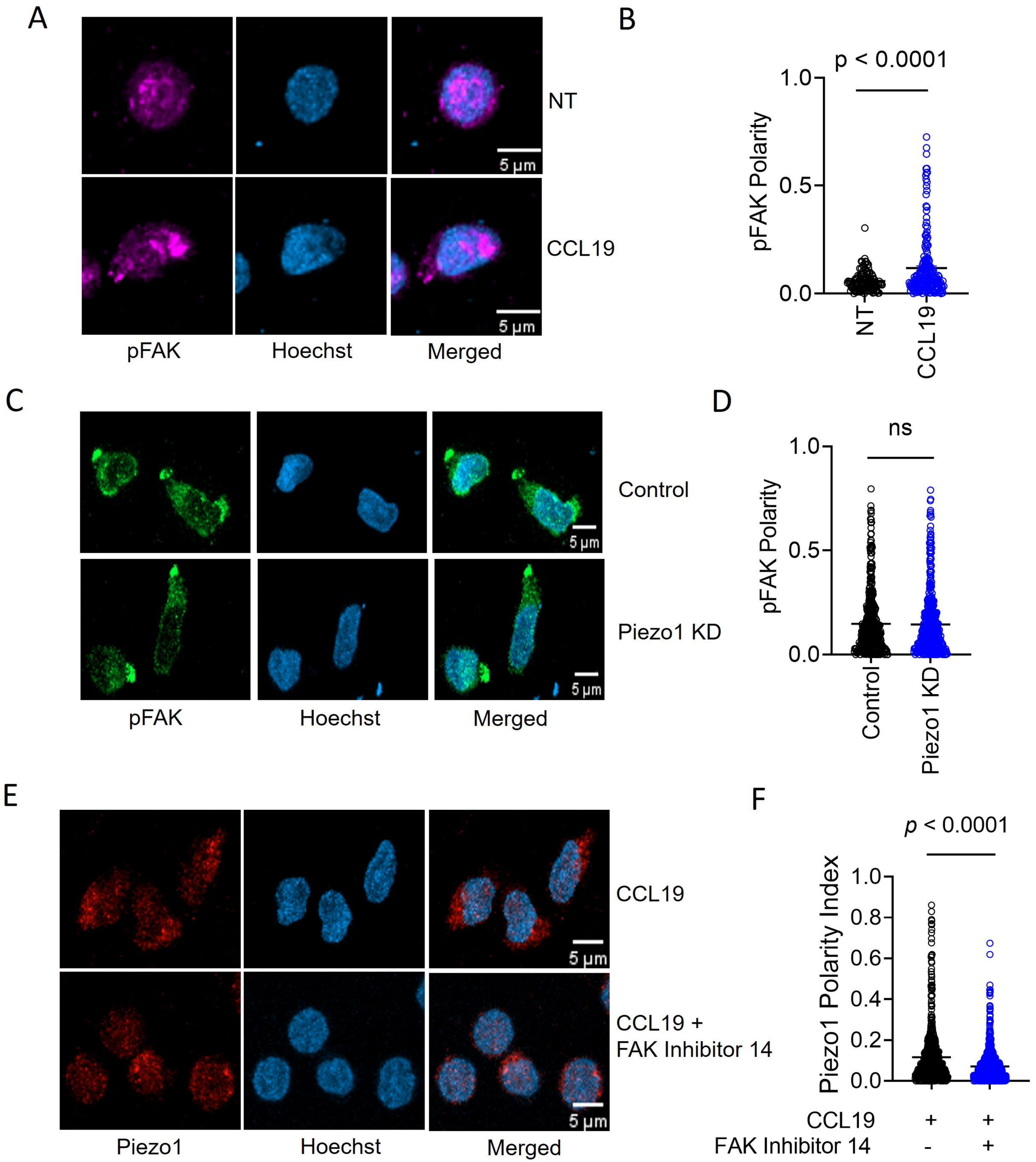
A
NT
CCL19
5 µm
pFAK
Hoechst
Merged
B
p < 0.0001
pFAK Polarity
1.0
0.5
0.0
NT
CCL19
C
Control
Piezo1 KD
pFAK
Hoechst
Merged
D
ns
pFAK Polarity
Control
Piezo1 KD
E
CCL19
CCL19 +
FAK Inhibitor 14
Piezo1
Hoechst
Merged
F
p < 0.0001
Piezo1 Polarity Index
1.0
0.8
0.6
0.4
0.2
0.0
CCL19 + +
FAK Inhibitor 14 - +

Figure 3

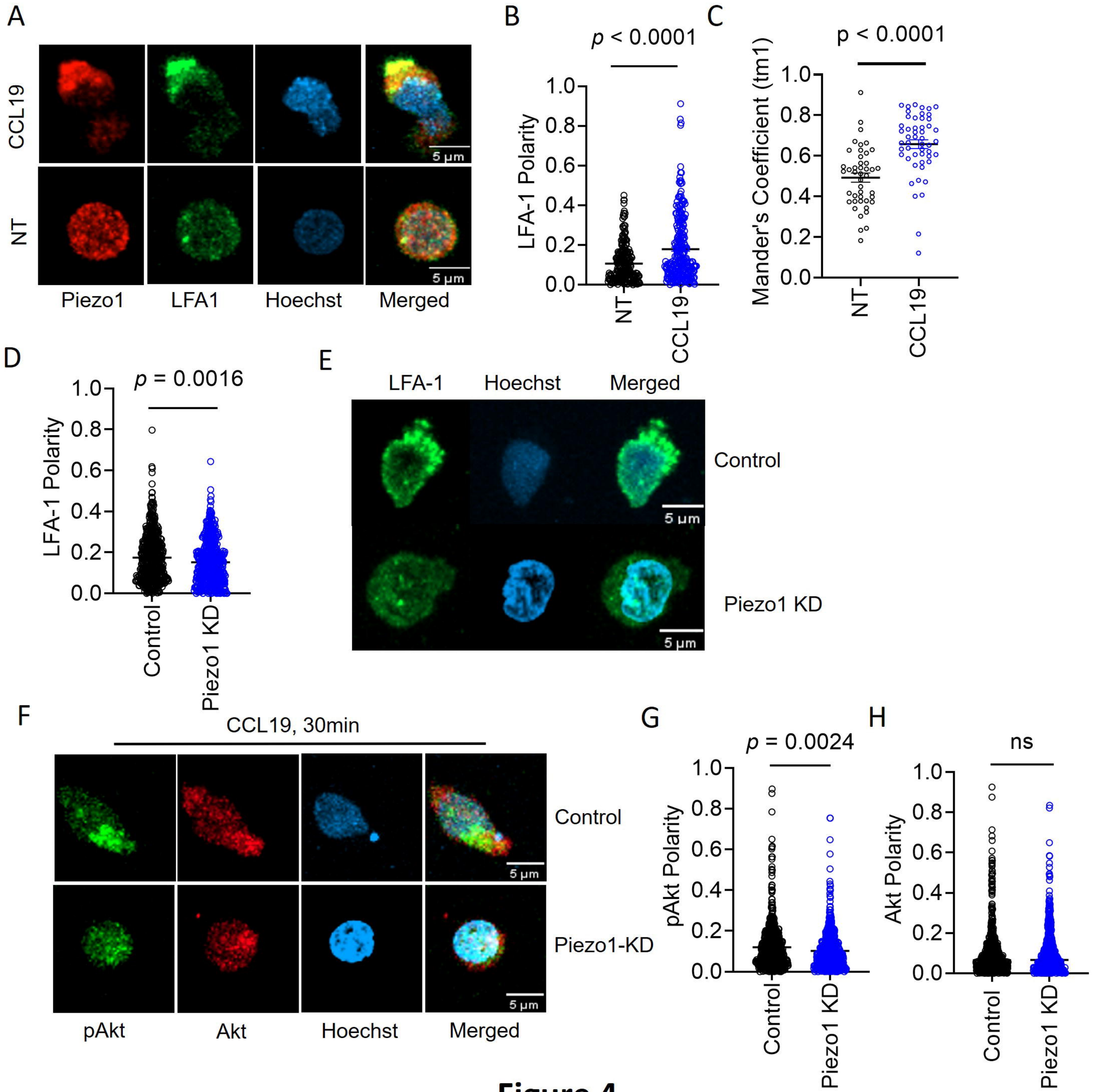
A
CCL19
NT
5 µm
5 µm
Piezo1
LFA1
Hoechst
Merged
B
p < 0.0001
LFA-1 Polarity
1.0
0.8
0.6
0.4
0.2
0.0
NT
CCL19
C
p < 0.0001
Mander's Coefficient (tm1)
1.0
0.8
0.6
0.4
0.2
0.0
NT
CCL19
D
p = 0.0016
LFA-1 Polarity
1.0
0.8
0.6
0.4
0.2
0.0
Control
Piezo1 KD
E
LFA-1
Hoechst
Merged
Control
Piezo1 KD
5 µm
5 µm
F
CCL19, 30min
Control
Piezo1-KD
5 µm
5 µm
pAkt
Akt
Hoechst
Merged
G
p = 0.0024
pAkt Polarity
1.0
0.8
0.6
0.4
0.2
0.0
Control
Piezo1 KD
H
ns
Akt Polarity
1.0
0.8
0.6
0.4
0.2
0.0
Control
Piezo1 KD

Figure 4

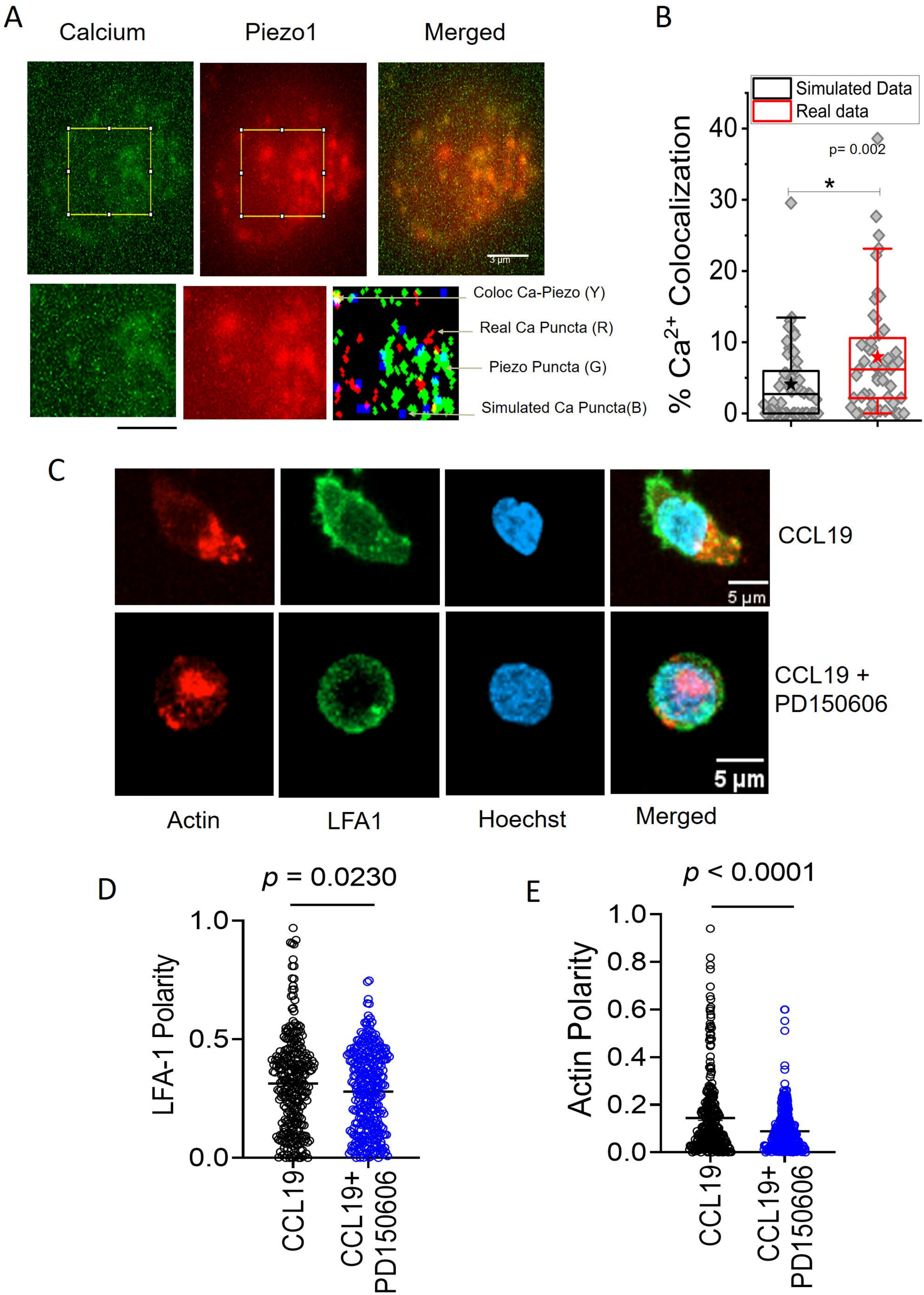
A
Calcium
Piezo1
Merged
3 µm
Coloc Ca-Piezo (Y)
Real Ca Puncta (R)
Piezo Puncta (G)
Simulated Ca Puncta(B)
B
Simulated Data
Real data
p= 0.002
*
% Ca2+ Colocalization
40
30
20
10
0
C
CCL19
5 µm
CCL19 +
PD150606
5 µm
Actin
LFA1
Hoechst
Merged
D
p = 0.0230
LFA-1 Polarity
1.0
0.5
0.0
CCL19
CCL19+
PD150606
E
p < 0.0001
Actin Polarity
1.0
0.8
0.6
0.4
0.2
0.0
CCL19
CCL19+
PD150606

Figure 5

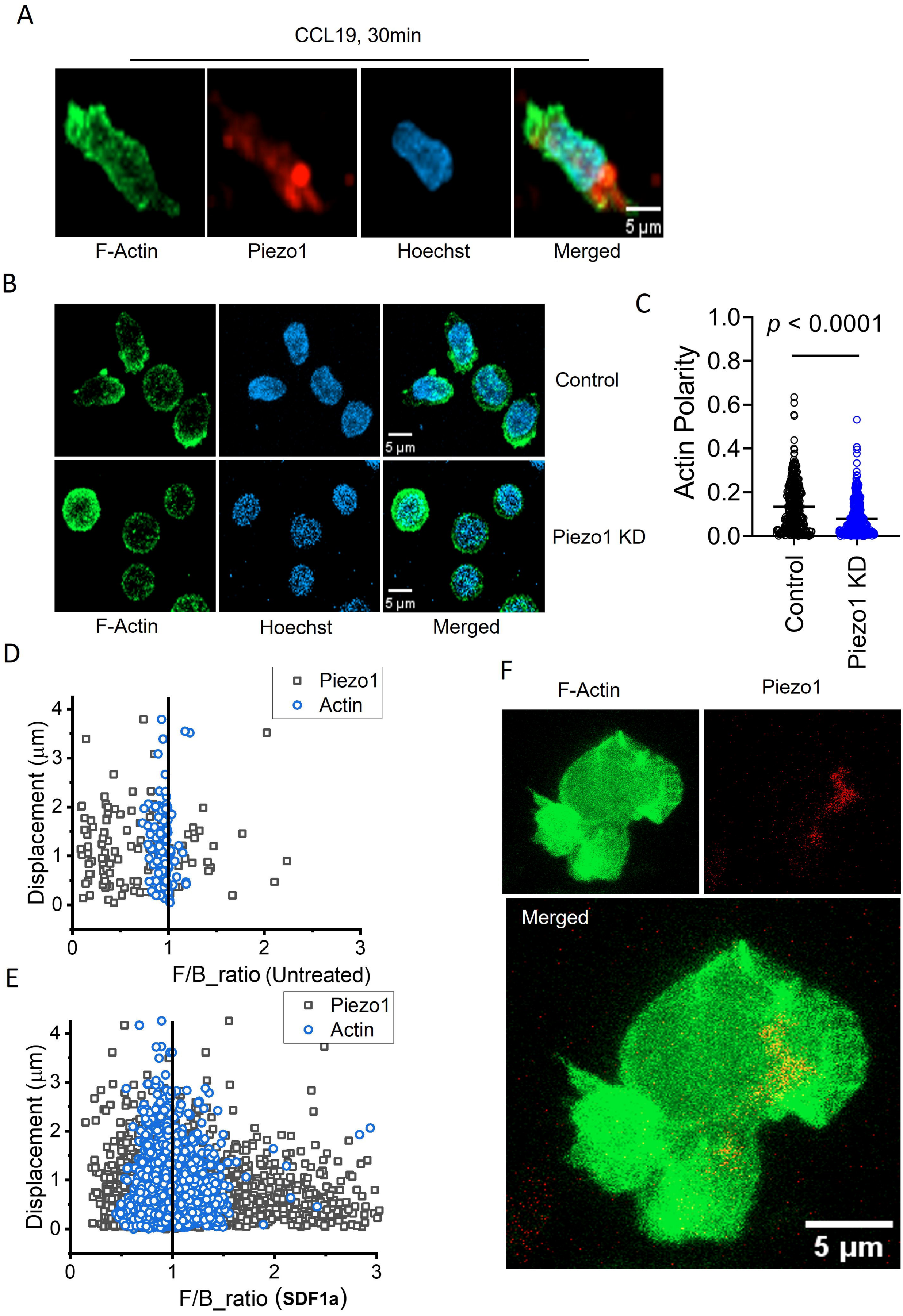
A
CCL19, 30min
F-Actin
Piezo1
Hoechst
Merged
5 µm
B
Control
Piezo1 KD
F-Actin
Hoechst
Merged
5 µm
C
p < 0.0001
Actin Polarity
1.0
0.8
0.6
0.4
0.2
0.0
Control
Piezo1 KD
D
Piezo1
Actin
Displacement (µm)
F/B_ratio (Untreated)
E
Piezo1
Actin
Displacement (µm)
F/B_ratio (SDF1a)
F
F-Actin
Piezo1
Merged
5 µm

Figure 6

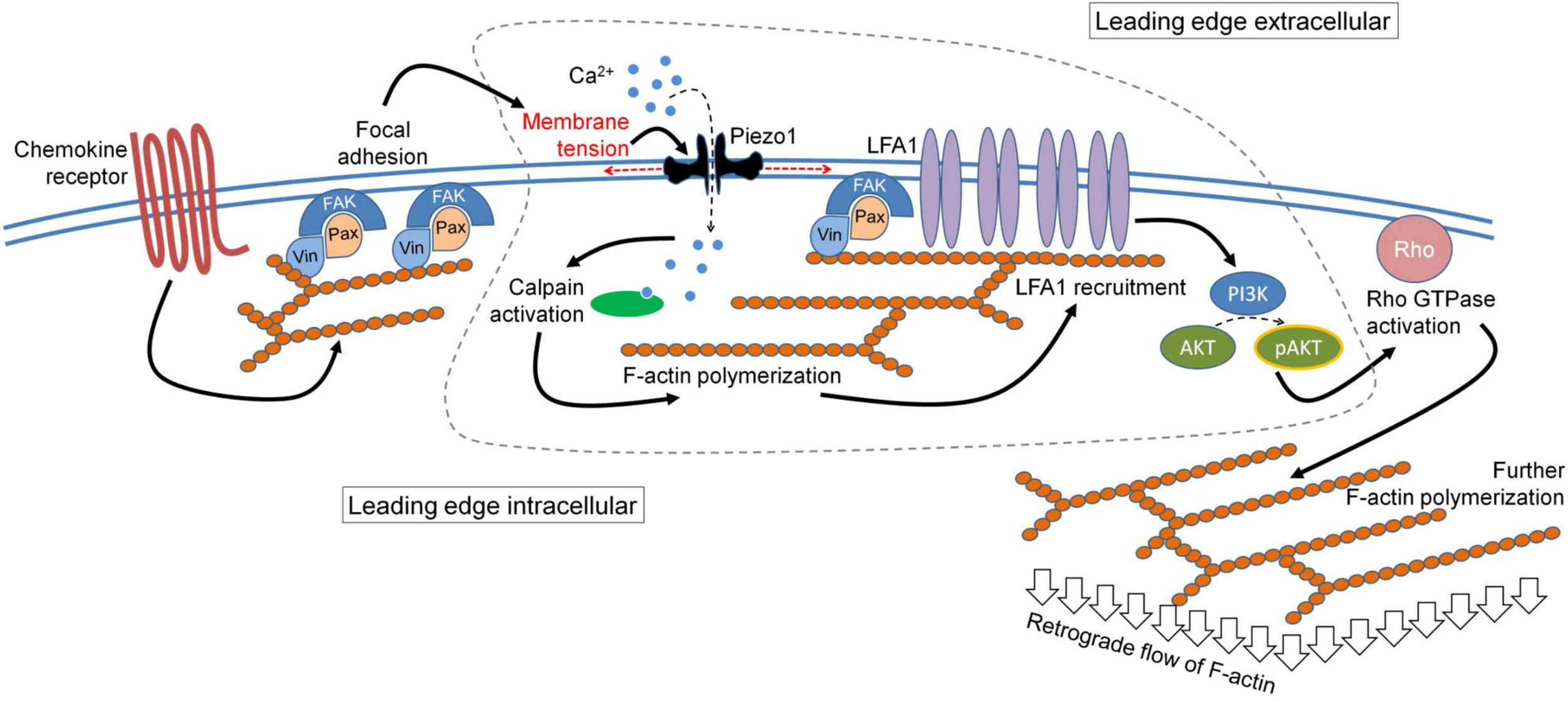
Leading edge extracellular
Ca2+
Chemokine receptor
Focal adhesion
Membrane tension
Piezo1
LFA1
FAK
Pax
Vin
FAK
Pax
Vin
FAK
Pax
Vin
Rho
Calpain activation
LFA1 recruitment
PI3K
Rho GTPase activation
AKT
pAKT
F-actin polymerization
Leading edge intracellular
Further F-actin polymerization
Retrograde flow of F-actin

Figure 7